Impact Source Localisation in Aerospace Composite Structures

Mario Emanuele DE SIMONE, Francesco CIAMPA, Salvatore BOCCARDI, Michele MEO

Mechanical Engineering Department, University of Bath, Bath, United Kingdom

Key words: Impact Localisation, acoustic emission, composite materials.

ABSTRACT

The most commonly encountered type of damage in aircraft composite structures is caused by low-velocity impacts due to foreign objects such as hail stones, tool drops and bird strikes. Often these events can cause severe internal material damage that is difficult to detect and may lead to a significant reduction of the structure's strength and fatigue life. For this reason there is an urgent need to develop structural health monitoring systems able to localise low-velocity impacts in both metallic and composite components as they occur.

This article proposes a novel monitoring system for impact localisation in aluminium and composite structures, which is able to determine the impact location in real-time without a-priori knowledge of the mechanical properties of the material. This method relies on an optimal configuration of receiving sensors, which allows linearization of well-known nonlinear systems of equations for the estimation of the impact location. The proposed algorithm is based on the time of arrival identification of the elastic waves generated by the impact source using the Akaike Information Criterion. The proposed approach was demonstrated successfully on both isotropic and orthotropic materials by using a network of closely spaced surface-bonded piezoelectric transducers. The results obtained show the validity of the proposed algorithm, since the impact sources were detected with a high level of accuracy. The proposed impact detection system overcomes current limitations of other methods and can be retrofitted easily on existing aerospace structures allowing timely detection of an impact event.

1 INTRODUCTION

In the last few years, both non-destructive evaluation (NDE) and Structural Health Monitoring (SHM) techniques were used for the localisation of acoustic emission (AE) sources due to impact events. Typically, the real-time knowledge of the impact location in metallic and composite materials is achieved through "passive techniques", in which ultrasonic transducers, fixed to the specimen surface or embedded into the structure, can be used to measure the impulsive material response [1].

A number of studies on the detection and localisation of impact sources are well documented in literature, many of them based on the triangulation technique, also known as "Tobias algorithm" [2]. In this methodology, the impact point is identified as the intersection of three circumferences, whose centres are the sensor locations. A triangulation technique can be used for isotropic and homogeneous structures, but it requires the accurate knowledge of the wave velocity that is assumed to be constant in all directions of propagation. Another approach based on the knowledge of the wave speed is the beamforming technique, which was originally introduced by McLaskey et al. [3] and then it was used by He et al [4]. This method is based on the use of a small array of sensors (from four to eight sensing elements) and on the delay-and-sum algorithm. Ciampa and Meo [5] proposed a modification of the triangulation technique in isotropic materials, which did not require the knowledge of the wave speed. However, the strong limitation of the above mentioned method is that they are not suitable for anisotropic and inhomogeneous materials. Kundu et al. [6],[7] developed an impact localisation technique to locate the impact source in isotropic and anisotropic plates. This algorithm, based on the minimization of an error function, or "objective function", was able to determine the impact coordinates by using four sensors, although the direction dependence of the wave velocity must be known in case of anisotropic media. Nakatani et al. [8] extended the beamforming technique to anisotropic structures with known velocity profile, whilst Seydel and Chang [9],[10] proposed a method based on the minimization of the difference between the actual and predicted response from piezoelectric sensors. Nevertheless, this technique required the knowledge of the mechanical properties of the medium and a theoretical model for the simulation of dynamic-acoustic behaviour

of the structure. Meo et al. [11], Kurokawa et al. [12], developed an algorithm for the impact point identification assuming an elliptical angular-group velocity pattern. This technique can be applied only to quasi-isotropic and unidirectional composite structures.

Since it is generally cumbersome to determine the information on group velocity of propagating waves in geometrically complex components and dispersive media, Ciampa and Meo [13],[14] and Kundu et al. [15],[16], developed impact localisation methods able to localise the acoustic source in an anisotropic plate using only six receiving sensors without the knowledge of the wave velocity. In Ciampa and Meo [13],[14] the impact coordinates and the wave velocities were obtained by solving a set of nonlinear equations through a combination of both local (Newton's) and global (unconstrained optimization) methods, whilst in Kundu et al. [15],[16] the acoustic source was localised from the intersection point of two direction lines generated by two clusters of sensors.

Another main issue of impact localisation methods is the estimation of the time of arrival (TOA) with high level of accuracy. The TOA, also called "onset time" of transient signals such as AE, seismograms or ultrasound signals, can be described as the moment when the ballistic wave originated at the impact source reaches one (or more) receiving sensor. The TOA is usually picked as the point where the first difference between the signal and the noise takes place. Several approaches were used in the past for automatic TOA estimation, many of them modified from seismology, due to the similarity between seismology and acoustic fields. The simplest method is to use an amplitude threshold picker, where the onset time is determined as the time corresponding a signal value immediately before the signal amplitude exceeds a particular threshold value [17]. The magnitude of the squared modulus of the continuous Wavelet transform (CWT) was used by Ciampa and Meo [5],[13],[14] to identify the TOA of the signals and then to calculate the time differences of arrival (TDOAs). However, CWT strongly depends on the selection of the mother wavelet, which may limit its use for structures with complex geometries. Another techniques called "Short Term Average (STA) / Long Term Average (LTA)" uses a dynamic threshold to discern the ballistic signal from the level of noise [18]. A number of algorithms based on the STA/LTA method can be found in literature,

however its poor accuracy in estimating the TOA was demonstrated in concrete structures [19]. Other techniques for the TOA estimation include cross-correlation [20],[21], energy criterion method, artificial neutral network [22], fractal dimension [23], spectrograms [24] and the Hinkley criterion [25]. Ciampa et al. [26],[27] proposed an alternative technique to the traditional TOA estimation method for acoustic source localisation on composite structures based on the reciprocal time reversal (TR) or inverse filtering (IF) technique. This approach was split into two steps. The first step consisted of recording and storing a set of signals representing a library of impulse responses from a number excitation points along the plane of the structure using a single surface-bonded receiving transducer. The second step consisted of a correlation between the impulsive transfer function associated with each excitation point and the inversion of the structural response of a new impact of unknown position. The maximum of the IF correlation coefficients corresponded to the impact point. However, this technology required an initial library of impulsive waveforms to be determined during the first step.

This paper starts from the research work of Ciampa and Meo for impact localisation on aluminium [5] and composite structures [13],[14] based on the TOA estimation. The proposed research work uses a different approach for the TOA estimation based on the Akaike Information Criterion (AIC) that, unlike traditional TOA estimation techniques, it allows identifying the onset time with high accuracy in the range of microseconds. Moreover the proposed research work provides a linearisation of the nonlinear system of equations to be solved. This would eliminate the dependence on the guess conditions for the identification of the impact coordinates. At the same time, the aim of this paper is to minimise the number of transducers, thus optimising the sensors configuration. The general assumption is that the composite material is homogeneous and anisotropic at the structural level. In strongly inhomogeneous media, the straight line propagation path of direct (ballistic) waves from the impact source to the receiver transducer could be interrupted by discontinuities (e.g. surface and subsurface flaws) that may alter the propagation path and generate wave scattering and reflections according to the Snell's law. However, this is not the case of this paper.

The outline of this research work is as follows: in Section 2, the linearised algorithm for the impact localisation is described. In Section 3, the Akaike Information Criterion is presented, with the description of two AIC pickers able to identify the TOA of a signal. Section 4 shows the set-up used to perform experimental tests, whilst in Section 5, all the impact localisation results are illustrated. The conclusions of this paper are presented in Section 6.

2 IMPACT LOCALISATION ALGORITHM

Let us consider an impact source point *I*, or a general acoustic emission source, at unknown coordinates (x_I, y_I) in the plane of the plate $x - y$. A number of n receiving transducers, are located at distance d_i $(i = 1, \dots, n)$ from the source. The origin of the Cartesian reference frame was arranged at the left bottom corner of the plate, whose dimensions are L, length, and W, width.

The coordinates of the impact source can be determined by solving the following general system of nonlinear equations [13],[14]:

$$\begin{cases} \|d_i\|^2 = (x_i - x_I)^2 + (y_i - y_I)^2 \\ t_i = \dfrac{\|d_i\|}{V_{g,i}} \end{cases} \qquad i = 1, \dots, n \tag{1}$$

where $V_{g,i}$ are the velocities of propagation of the stress wave reaching the i^{th} transducer, t_i are the times of detection of the AE signals and (x_i, y_i) are the coordinates of the i^{th} sensor.

Combining both terms of (1) it is possible to obtain a number of n equations in the form of:

$$(x_i - x_I)^2 + (y_i - y_I)^2 - \left(t_i V_{g,i}\right)^2 = 0 \qquad i = 1, \dots, n \tag{2}$$

which is the equation of a circumference with radius ${r_i}^2 = \left(t_i V_{g,i}\right)^2$. We have a system of n nonlinear equations for $2(n + 1)$ unknowns (i.e. n velocities, n times of arrival and two source coordinates). Considering one of the sensor as "reference sensor", it is possible to relate the travel time required to reach this sensor, t_{ref}, and the time differences of arrival between other sensors and the reference one, $\Delta t_{ref,j}$, obtaining an expression for the time of arrival concerning the j^{th}, sensor:

$$t_j = t_{ref} \pm \Delta t_{ref,j} \qquad j = 1, \dots, n - \{ref\} \tag{3}$$

Substituting (3) into (2), it becomes:

$$\begin{cases} (x_j - x_I)^2 + (y_j - y_I)^2 = [(t_{ref} \pm \Delta t_{ref,j}) V_{g,j}]^2 \\ (x_{ref} - x_I)^2 + (y_{ref} - y_I)^2 = (t_{ref} V_{g,ref})^2 \end{cases} \qquad j = 1, \dots, n - \{ref\} \qquad (4)$$

Considering TDOAs as determined by using an appropriate TOA estimation method, the number of unknowns is equal to $n + 3$ (i.e. n velocities, the time of arrival of the reference sensor and two source coordinates). Our aim is to reduce the number of surface-bonded transducers up four sensors. Since system (4) can only be solved if the number of variables is equal to the number of equations, an optimal sensor configuration is necessary to solve the system of equations. The main idea is to locate the four sensors relatively close together (see Figure 1), so that they experience the same propagation velocity $(V_{g,i} = V_g)$. With this assumption system (4) becomes:

$$\begin{cases} (x_j - x_I)^2 + (y_j - y_I)^2 = [(t_{ref} \pm \Delta t_{ref,j}) V_g]^2 \\ (x_{ref} - x_I)^2 + (y_{ref} - y_I)^2 = (t_{ref} V_g)^2 \end{cases} \qquad j = 1, \dots, 4 - \{ref\} \qquad (5)$$

System (5) consists of four equations for four unknowns, $\{\boldsymbol{x}\} = \{x_I, y_{I,} t_{ref}, V_g\}$ and its resolution, after a suitable linearisation, is the topic of next sub-section.

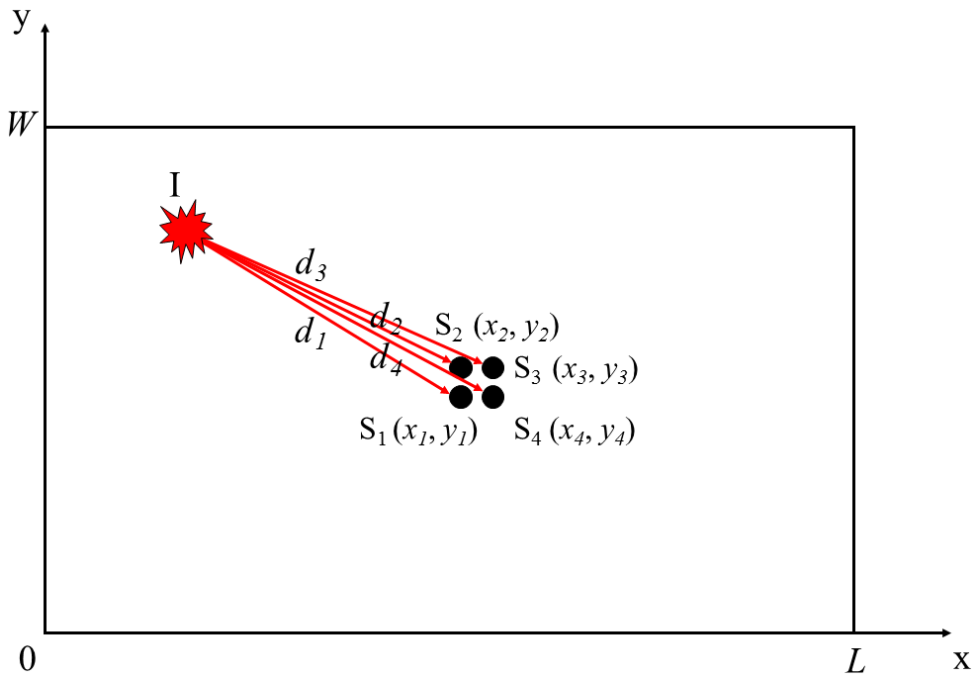

Figure 1. Sensor arrangement for the source location.

2.1 LINEARISATION PROCESS

Subtracting the reference sensor equation from other equations in (5), the following system of equations is obtained:

$$\begin{aligned} {x_j}^2 - {x_{ref}}^2 - 2x_j x_I + 2x_{ref} x_I + {y_j}^2 - {y_{ref}}^2 - 2y_j y_I + 2y_{ref} y_I \\ = {V_g}^2 \Delta t_{ref,j} \left(2t_{ref} + \Delta t_{ref,j}\right) \end{aligned} \tag{6}$$

Considering the known quantities $b_j = \left({x_j}^2 + {y_j}^2\right) - \left({x_{ref}}^2 + {y_{ref}}^2\right)$, equations (6) become:

$$b_j - 2\left[x_I\left(x_j - x_{ref}\right) + y_I\left(y_j - y_{ref}\right)\right] - {V_g}^2 \Delta t_{ref,j}\left(2t_{ref} + \Delta t_{ref,j}\right) = 0 \tag{7}$$

It is possible to use the following positions for the known differences between sensors coordinates, $x_{ref,j} = x_j - x_{ref}$ and $y_{ref,j} = y_j - y_{ref}$, so that equations (7) can be written as:

$$b_j - 2\left[x_I x_{ref,j} + y_I y_{ref,j}\right] - {V_g}^2 \Delta t_{ref,j}\left(2t_{ref} + \Delta t_{ref,j}\right) = 0 \tag{8}$$

Rearranging equations (8), they become:

$$x_I x_{ref,j} + y_I y_{ref,j} + {V_g}^2 t_{ref} \Delta t_{ref,j} = \frac{b_j}{2} - {V_g}^2 \frac{{\Delta t_{ref,j}}^2}{2} \tag{9}$$

which in matrix form, assuming sensor 1 as the reference sensor, can be expressed as:

$$\begin{bmatrix} x_{1,2} & y_{1,2} & \Delta t_{1,2} \\ x_{1,3} & y_{1,3} & \Delta t_{1,3} \\ x_{1,4} & y_{1,4} & \Delta t_{1,4} \end{bmatrix} \begin{Bmatrix} x_I \\ y_I \\ {V_g}^2 t_1 \end{Bmatrix} = \frac{1}{2} \begin{Bmatrix} b_2 \\ b_3 \\ b_4 \end{Bmatrix} - \frac{{V_g}^2}{2} \begin{Bmatrix} {\Delta t_{1,2}}^2 \\ {\Delta t_{1,3}}^2 \\ {\Delta t_{1,4}}^2 \end{Bmatrix} \tag{10}$$

or, in general, as reported below:

$$[A]\{\boldsymbol{x}\} = \{B\} - {V_g}^2 \{C\} \tag{11}$$

The variables vector is expressed by:

$$\{\boldsymbol{x}\} = [A]^{-1}\{B\} - {V_g}^2 [A]^{-1}\{C\} \tag{12}$$

Considering the following positions, $a_k = [A]^{-1}\{B\}|_k$ and $c_k = [A]^{-1}\{C\}|_k$, with $k = 1, 2, 3$, we achieve:

$$\begin{Bmatrix} x_I \\ y_I \\ {V_g}^2 t_1 \end{Bmatrix} = \begin{Bmatrix} a_1 \\ a_2 \\ a_3 \end{Bmatrix} - {V_g}^2 \begin{Bmatrix} c_1 \\ c_2 \\ c_3 \end{Bmatrix} \tag{13}$$

The final expressions for the four unknowns are:

$$\begin{cases} x_I = a_1 - {V_g}^2 c_1 \\ y_I = a_2 - {V_g}^2 c_2 \\ {V_g}^2 t_1 = a_3 - {V_g}^2 c_3 \end{cases} \quad (14)$$

Substituting expressions (14) in the reference sensor equation in (5) and after some mathematical manipulation, a final third order equation, with reference time of arrival, t_1, as only unknown, is formulated as follows:

$$ {t_1}^3 Z_1 + {t_1}^2 Z_2 + t_1 Z_3 + Z_4 = 0 \quad (15)$$

where Z_i coefficients are combinations of known quantities that for clarity reasons are reported in the Appendix.

Although (15) admits three possible solutions, only one of them is physically feasible, whereas the other two should be discarded. After obtaining t_1 from (15), the propagation velocity can easily be calculated using the following equation, coming from the third of (14):

$$V_g = \sqrt{\frac{a_3}{t_1 + c_3}} \quad (16)$$

Finally it is possible to obtain the values of the impact coordinates substituting (16) in the first two equations in (14).

3 AKAIKE INFORMATION CRITERION METHOD

Since the inputs of the proposed algorithm are the time differences of arrival, a suitable approach for time of arrival estimation needs to be chosen. In this research work the onset time determination is based the Akaike Information Criterion [27]-[30].

The main assumption for AIC is to consider the signal, or a general time series, as divided in two different locally stationary segments [31], each modelled as an autoregressive (AR) process. The first segment is the non-informative part, and it is called “noise”, while the second one is the informative part, and it is called “signal”. These two datasets are separated by the onset time. The AIC, derived by [27], is represented by the following equation:

$$AIC = -2\ln(L) + 2P \tag{17}$$

where P is the number of parameters in the statistical model, and L is the maximized value of the likelihood function for the estimated model. Originally the optimal order for an AR process fitting a time series was determined by using function (17).

When there are several competing models, the minimum AIC estimation (MAICE) is defined by the model which give the minimum of AIC function [30]. The model is established by a mathematical method illustrated by Kitagawa and Akaike [31].

A time series $\{x_1, x_2, \dots, x_n\}$ can be divided into two segments $(j = 1, 2)$, $\{x_1, x_2, \dots, x_k\}$ and $\{x_{k+1}, x_2, \dots, x_n\}$ where k indicates the point whose corresponding time is the unknown onset time. Both segments could be expressed by:

$$x_i = \sum_{m=1}^{M} a_m^j \, x_{i-m} + e_i^j \qquad j = 1, 2 \tag{18}$$

where M is the order and a_m^j are the coefficients of the AR process used to model the two datasets. Furthermore $i = M + 1, \dots, k$ for interval $j = 1$, and $i = k + 1, \dots, n - M$ for $j = 2$.

Both time series are divided into a deterministic and a non-deterministic part, e_i^j, the second one considered as a Gaussian white noise, with mean zero, variance σ_j^2 and uncorrelated with the deterministic part. The non-deterministic part of the time series in two intervals can be extracted by using the maximum likelihood estimation (MLE).

Considering the previous hypothesis about the noise model, it is possible to express the joint density function of all variables e_i^j, considered as fixed parameters, through the approximate likelihood function L:

$$L(\Theta_j, k, M|x) = \prod_{j=1}^{2} \left(\frac{1}{\sigma_j^2 2\pi}\right)^{n_j/2} \exp\left[-\frac{1}{2\sigma_j^2} \sum_{i=p_j}^{q_j} \left(x_i - \sum_{m=1}^{M} a_m^j \, x_{i-m}\right)^2\right] \tag{19}$$

where $\Theta_j = \Theta_j(a_1^j, \dots, a_m^j, \sigma_j^2)$ represents the model parameters, $p_1 = M + 1$, $p_2 = k + 1$, $q_1 = k$, $n_1 = k - M$, $n_2 = n - k - M$.

By using MLE it is possible to find the values of the model parameters that make the observed results the most probable, the same that maximize the equation (19). Considering the logarithm of equation (19) and searching for the MLE of the model parameters we obtain:

$$\frac{\partial \ln L}{\partial \Theta_j} = 0 \tag{20}$$

whose solution can be expressed as:

$$\sigma^2_{j,\max} = \frac{1}{n_j} \sum_{i=p_j}^{q_j} \left(x_i - \sum_{m=1}^{M} a_m^j \, x_{i-m} \right)^2 \tag{21}$$

It is simple to obtain the maximized logarithmic likelihood function inserting equation (21) into equation (19):

$$\ln L = -\frac{k-M}{2} \ln \sigma^2_{1,\max} - \frac{n-k-M}{2} \ln \sigma^2_{2,\max} + C_1 \tag{22}$$

where C_1 is a constant. Equation (22) is the basis for equation (17). In the case of fixed M order, as in current application, AIC function is a measure for the model fit. k point where AIC is minimized, or equivalently L is maximized, indicates the optimal separation of the two time series and the corresponding time value is regarded as the onset time of the signal [32],[33].

Considering AIC as function of merging point *k*, we have the AR-AIC picker expressed by the following equation:

$$AIC(k) = (k-M) \ln \sigma^2_{1,\max} + (n-k-M) \ln \sigma^2_{1,\max} + C_2 \tag{23}$$

where C_2 is a constant. It is possible to calculate the AIC function directly from the signal without using the AR coefficients, considered that for the AR-AIC picker the order M of the AR process must be specified by trial and error and the AR coefficients have to be calculated for both intervals. Considering $M \ll n$ and constant C_2 as a negligible quantity if n is large enough, equation (23) is simplified in the Maeda's relation [34]:

$$AIC(k) = k \ln\big(\mathrm{var}(x[1,k])\big) + (n-k-1) \ln\big(\mathrm{var}(x[k+1,n])\big) \tag{24}$$

where k represents the range through all points of the signal and $\mathrm{var}(\cdot)$ is the sample variance.

AIC function (24) is the basis equation for the methods used in this research work.

After computation of AIC function, it is necessary to calculate its global minimum. The relative time value can be considered the time of arrival of the signal. It should be noted that for the TOA calculation only a part of the time series containing the onset time should be considered. The selection of this time window and the signal-to-noise (S/N) ratio determine the accuracy of TOA.

3.1 PREVIOUS AIC PICKERS

Several procedures were presented in literature to manage the two related problems: a proper choice of the time window and the appropriate signal to use in the algorithm, dependent on the S/N ratio of the original signal. They generally depend on the application field: e.g. seismology [32]-[36] and acoustic [19],[37]-[40]. There are many similarities between acoustic emissions and seismograms, however a number of differences are present, as the fact that in seismology the signal and the noise are usually located in different frequency range. In this case it is possible to obtain reliable results eliminating the noise through a simple Fourier transform and corresponding filter. AE signal and noise are often in the same frequency range (20-500 kHz) with a consequent variable signal-to-noise ratio. A signal would be influenced unavoidably after an inadequate filtering, with incorrect time of arrival results as principal consequence [41]. Therefore it is necessary to diminish the noise as much as possible instead of eliminating it, by using, for example a Butterworth filter, whose characteristics are dependent on considered signal.

In seismology, Zhang et al. [33] applied the AIC picker to detect the *P*-wave arrival using the time window chosen by the discrete wavelet transform, acting to single-components seismograms through a series of sliding time windows. For AE in concrete, Kurz et al. [19] applied an adapted automatic AIC picker based on (24), considering two particular signal-envelopes instead of signal: the complex wavelet transform and Hilbert transform; the time window was chosen after the determination of a first onset, obtained by using a constant threshold value on the squared and normed signal-envelope.

In this research work two different AIC pickers are considered, here referred as “characteristic function AIC picker” [37],[38] and “threshold AIC picker”[39],[40]. They are described in Sections 3.2 and 3.3 respectively.

3.2 CHARACTERISTIC FUNCTION AIC PICKER

3.2.1 Choice of characteristic function

The first considered AIC picker is based on a suitable mathematical function, called “characteristic function” (CF), whose purpose is to improve the resolution level between noise and signal through the enhancement of changes in signal features [42] such as the frequency, the amplitude or both. In correspondence of these changes, it is possible to detect the time of arrival of the signal. For this reason the performance of the picker highly depends on the chosen characteristic function. Among all characteristic functions used in literature, it is possible to remember the functions that enhances the signal amplitude changes: the absolute value function $F(i) = |x(i)|$, the square function $CF(i) = x(i)^2$, the envelope of the signal calculated by Hilbert transform and the squared envelope. The principal limitation is that these function are not sensitive to periodic signal changes, very useful if a low signal-to-noise ratio signal is considered. To overcome this limitation frequency-sensitive functions need to be chosen, such as the Allen’s function, a squared polynomial function used for a seismogram threshold picker [42]:

$$CF(i) = x(i)^2 + R_1\big(x(i) - x(i-1)\big)^2 \tag{25}$$

where $R_1\big(x(i) - x(i-1)\big)^2$ represents changes in frequency, with R_1 as a weighting constant dependent on the signal. Despite equation (25) is suitable for changes in amplitude and frequency, it can be used effectively for bulk specimens and not for thin plates. Because of it is a square function, it can suppress the amplitude of the first and weaker mode, much lower respect to the amplitude of the second mode if a thin plate is considered. In this research work the following characteristic function, suitable for thin plate, is chosen:

$$CF(i) = |x(i)| + R_2|x(i) - x(i-1)| \quad (26)$$

where R_2 is a constant set to $R_2 = 4$ for thin-plate specimens in accordance to [37],[38].

3.2.2 AIC picker algorithm

The algorithm is divided into two steps (Figure 2), consisting of a first rough estimation of the onset time during the first step, with a more precise determination of it during the second step. The first step starts with the determination of a shortened time window. The starting time was set at the beginning of the original signal within the noise level and considered a non-informative part. The ending time was set after the global maximum of the characteristic function (26), t_{MAX}, on time $t_{\mathrm{MAX}} + \Delta t_{AM}$. The time delay Δt_{AM} is a value depending on the tested material, set to 20 µs for our experiment. Maeda's relation (24), with the characteristic function (26) as input, is applied on this time window and the first onset time, t_{MIN}, is determined. The aim of the second step is to increase the accuracy of the AIC picker by focusing on the neighbourhood of the first estimation. A new time window is considered, whose limits are $t_{\mathrm{MIN}} - \Delta t_{FB}$ and $t_{\mathrm{MIN}} + \Delta t_{FA}$, where the setting are $\Delta t_{FB} = 30$ µs and $\Delta t_{FA} = 10$ µs. A new application of (24) on this new time window defines the actual time of arrival.

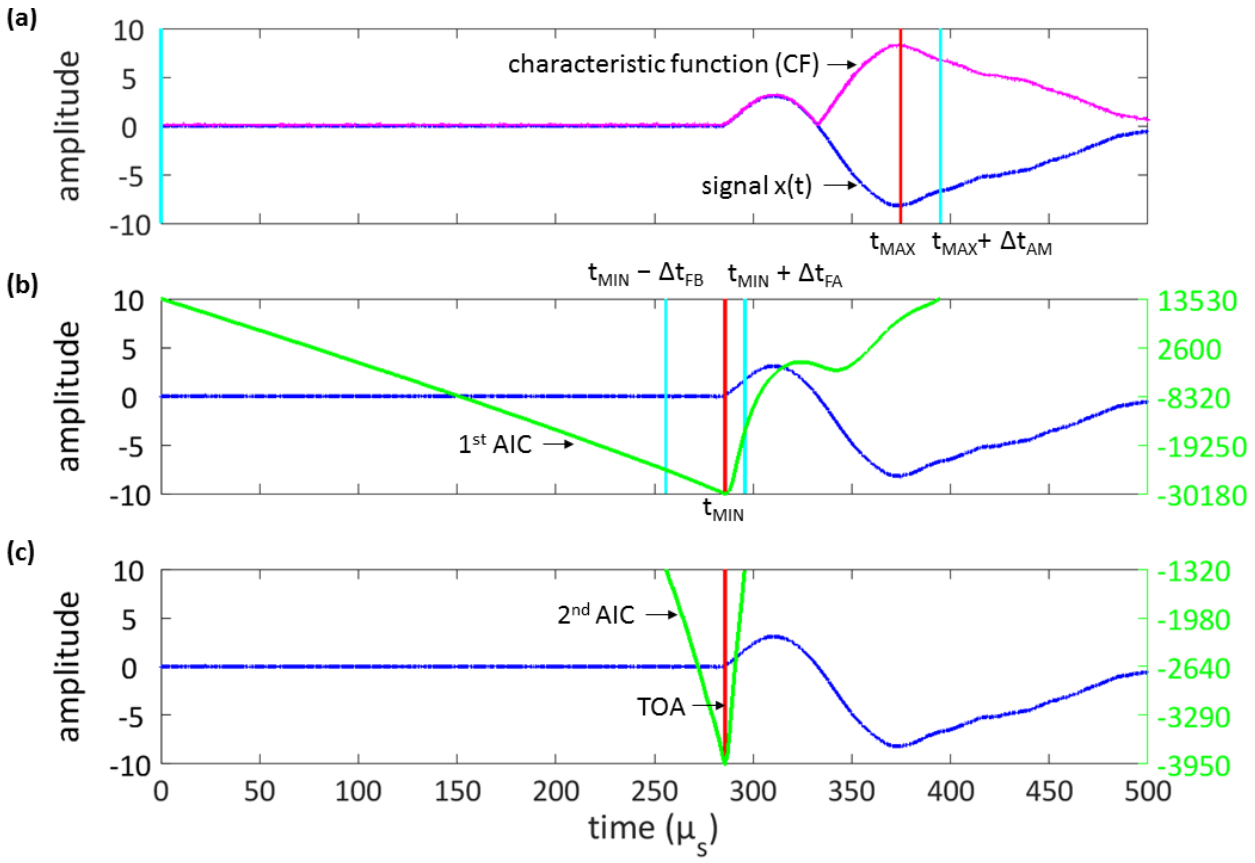

Figure 2. Visual description of CF-AIC picker: (a) determination of the initial time window; (b) estimation of the first TOA and determination of the second time window; (c) estimation of the final TOA.

3.3 THRESHOLD AIC PICKER

The second considered AIC picker is, as the first one, a two-step process (Figure 3). The structure of the steps is very similar to the previous AIC picker, but in this case it is not necessary a characteristic function.

During the first step, Maeda's relation (24), with the original signal as input, is applied on a shortened time window that is determined by using the following threshold amplitude level:

$$\left(\sum_{i=k+1}^{10}|x(i)|\right)\Big/10 \geq T\left(\sum_{i=1}^{k}|x(i)|\right)\Big/k \qquad (27)$$

where there is a comparison between the mean amplitude of a shifting set of 10 data [left part of (27)] and the mean amplitude of the interval of the time series ranging from 1 to k multiplied by a constant T depending on the signal [right part of (27)]. The ending of time window is set at the time t_0

corresponding to the first value k_0 that satisfies expression (27). The first estimation of the onset time t_1 is determined considering the interval $[0, t_0]$.

The second step considers a time window centred in t_1 with a length of $2\Delta k$, where Δk depends on the sample frequency. For our purpose, a variant of this method, that considers a length of $2(t_1 - t_0)$ for the second time window, is used [40]. A new application of (24) on this new time window defines the actual time of arrival.

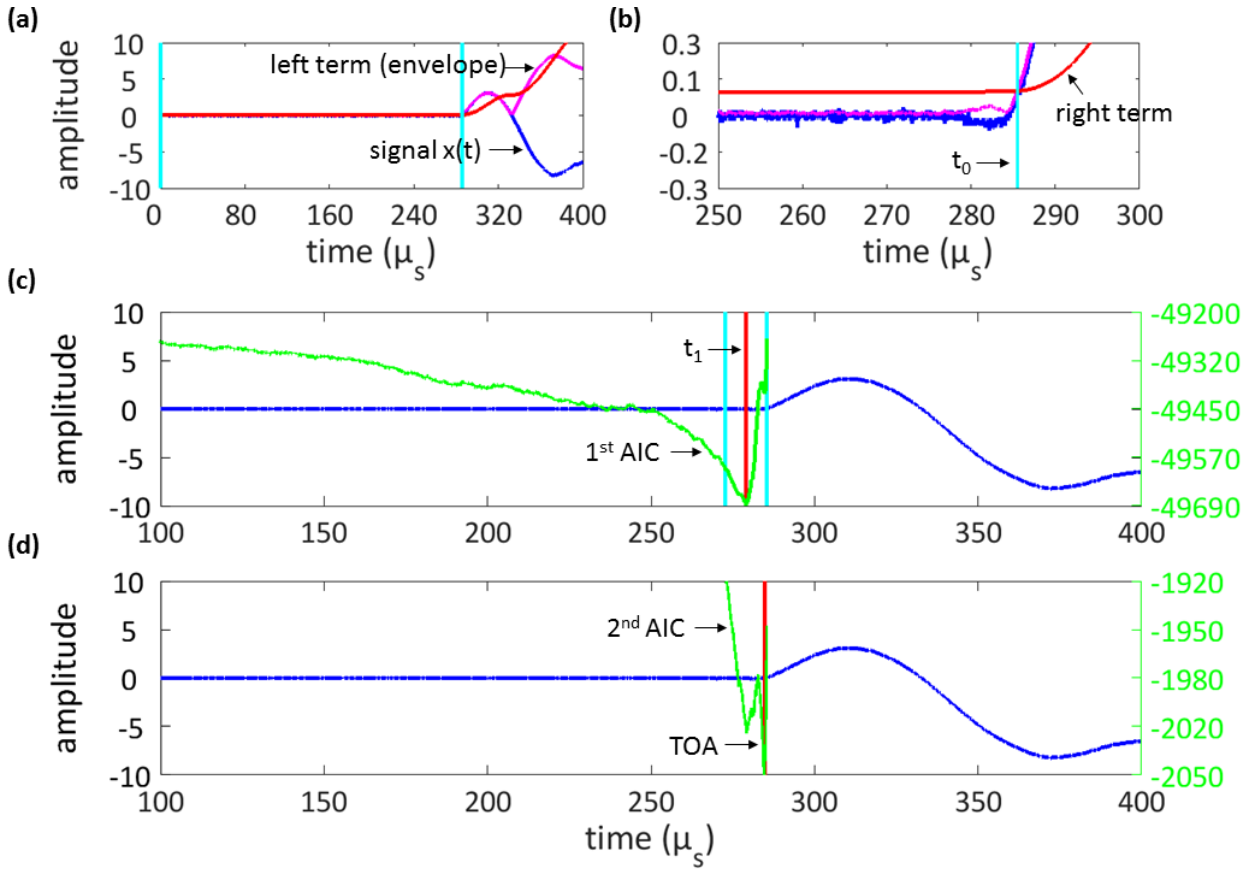

Figure 3. Visual description of threshold AIC picker: (a) determination of the initial time window [left term refers to formula (27)]; (b) zoom on onset time zone [right term refers to formula (27)]; (c) estimation of the first TOA and determination of the second time window; (d) estimation of the final TOA.

4 EXPERIMENTAL SET-UP

To validate the described algorithms, experimental impact location tests were conducted on two different structures (see Figure 4 and Figure 5):

- an aluminium plate with dimensions $350 \times 260 \times 8$ mm^3;
- a carbon fibre reinforced plastic (CFRP) plate with dimensions $290 \times 290 \times 5$ mm^3.

The impacts were generated by using an aluminium ball dropped from a defined height so that the same impact energy was achieved. The impulsive waveforms were measured employing four surface-bonded piezoelectric transducers (PIC 255) with diameter of 6.5 mm and thickness of 0.3 mm. By considering the small dimensions of sensors (e.g. the maximum diameter was 6.5 mm), the squared configuration shown in Figure 1 was assumed as the most suitable among all possible geometries, so that the transducers could be relatively close together. Other configurations and geometries would have not fulfilled the fundamental condition that all receiver transducers will experience the same group velocity. The signals were acquired using a four-channel oscilloscope with 16 bits of resolution, a sampling rate of 20 MHz and an acquisition window of 5 ms. A MATLAB software code implemented by the authors was written to analyse the waveforms for finding the TOA and the impact location by using the linearised algorithm. Sensor locations are reported in Table 1. The Cartesian reference frame was chosen with the origin at the bottom left corner of the specimens.

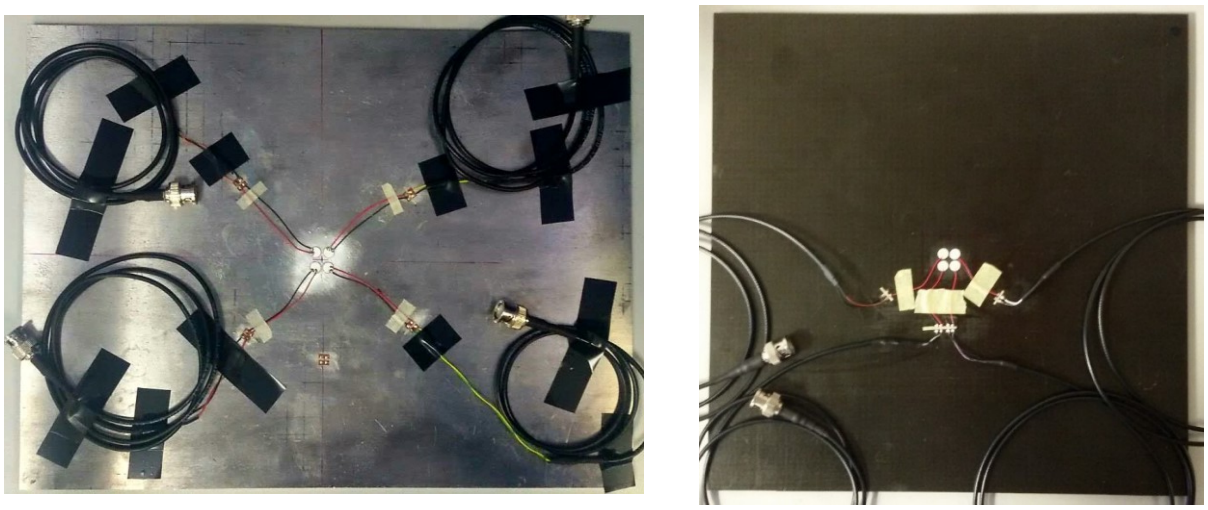

Figure 4. Considered specimens: aluminium plate (left), composite plate (right).

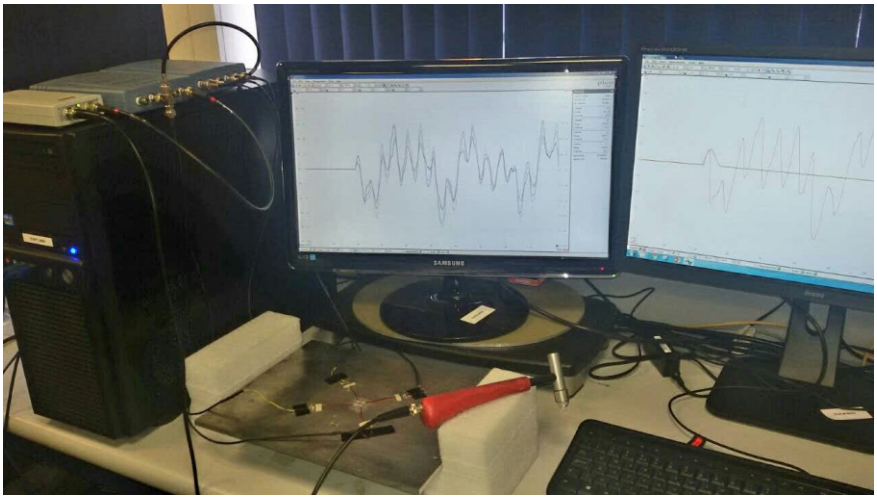

Figure 5. Experimental set-up.

Table 1. Sensor coordinates on the considered specimens.

	Aluminium		Composite	
	x-Coordinate (mm)	y-Coordinate (mm)	x-Coordinate (mm)	y-Coordinate (mm)
Sensor 1	177	126	142	135
Sensor 2	176	134	142	142
Sensor 3	185	134	149	142
Sensor 4	184	126	149	135

5 IMPACT LOCALISATION RESULTS

Table 2 and Figure 6 shows an example of TOA calculation, considering Impact 1 on the aluminium plate and the threshold AIC picker.

Table 2. TOA results – Impact 1 and threshold AIC picker (aluminium plate).

	TOA_{S1} (μs)	TOA_{S2} (μs)	TOA_{S3} (μs)	TOA_{S4} (μs)
Impact 1	933.6	930.52	930.3	933.78

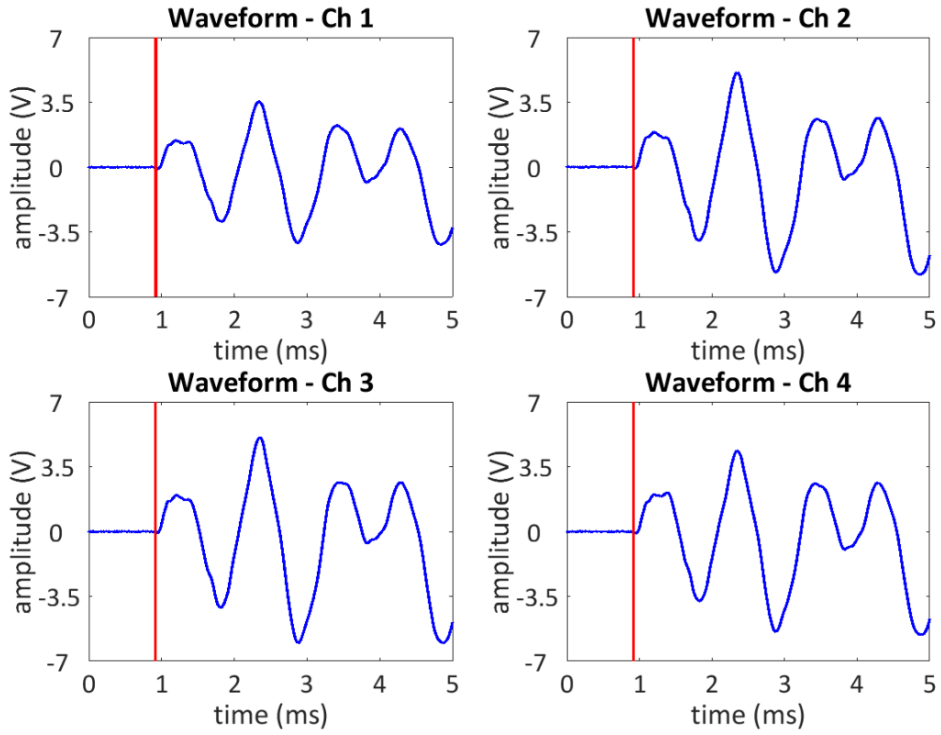

Figure 6. Acquired signals and calculated TOAs – Impact 1 and threshold AIC picker (aluminium plate).

Since the receiving sensors are very close each other, the TOAs are of the order of microseconds. The absolute TOA differences obtained by using both AIC picker methods described in Section 3 are reported in Table 3.

Table 3. Absolute TOA differences using both AIC pickers.

	Sensor 1 (μs)		Sensor 2 (μs)		Sensor 3 (μs)		Sensor 4 (μs)	
	Aluminium	Composite	Aluminium	Composite	Aluminium	Composite	Aluminium	Composite
Impact 1	4.14	5.19	4.1	5.2	4.1	5.2	4.14	5.19
Impact 2	6.88	7.07	6.83	6.9	6.87	6.91	6.93	7.07
Impact 3	6.12	9.21	6.12	9.09	6.12	9.22	6.12	9.26
Impact 4	7.23	9.05	7.24	9.04	7.23	9.04	7.23	9.05
Impact 5	5.42	8.17	5.42	8.07	5.44	7.93	5.42	8.07
Impact 6	6.42	5.81	6.42	5.8	6.42	5.8	6.36	5.81
Impact 7	5.09	20.74	5.09	20.75	5.01	20.77	5.04	20.76
Impact 8	5.57	19.07	5.59	19.06	5.54	19.06	5.5	19.06
Impact 9		9.77		9.7		9.55		9.63

As it can be seen in Table 3, the maximum difference in TOAs is less than 21 μs. Figure 7 and Figure 8 show the source localisation results considering the two specimens, whilst Table 4 and Table 5 depict the evaluated impact position and the location error as expressed by the following formula [43]:

$$\Psi = \sqrt{(x_{real} - x_{calculated})^2 + (y_{real} - y_{calculated})^2} \tag{28}$$

where (x_{real}, y_{real}) are the coordinates of the real impact position and $(x_{calculated}, y_{calculated})$ are the coordinates of the impact location using the described algorithm.

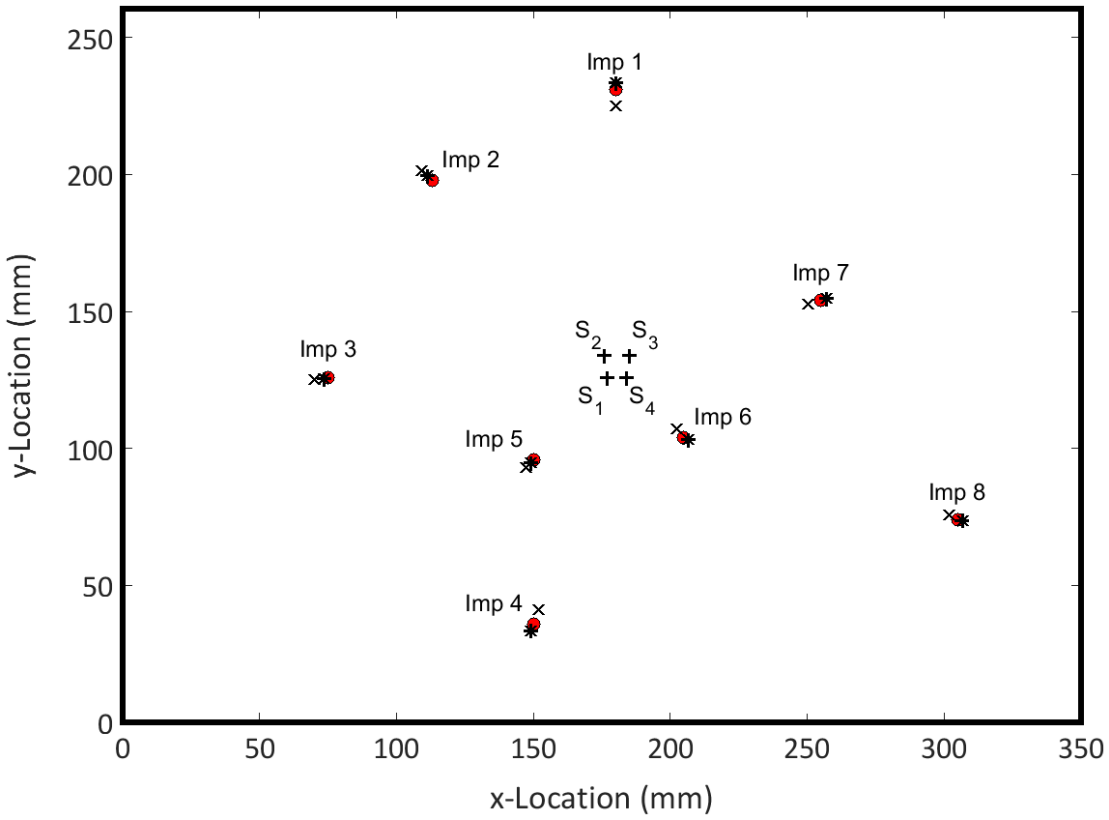

Figure 7. Source location results on the aluminium plate. The calculated impact positions are shown as a cross (×) for the CF-AIC picker, and as a star (∗) for the threshold AIC picker. The true impact positions are shown as a circle (∘).

Table 4. Impact positions and errors for the aluminium plate.

	X (mm, real value)	X (mm, detected value – CF AIC picker)	X (mm, detected value – threshold AIC picker)	Y (mm, real value)	Y (mm, detected value – CF AIC picker)	Y (mm, detected value – threshold AIC picker)	Location error Ψ (mm, CF AIC picker)	Location error Ψ (mm, threshold AIC picker)
Impact 1	180	180.1	180.13	231	225.09	233.35	5.91	2.35
Impact 2	113	109.35	111.36	198	201.44	199.51	5.02	2.23
Impact 3	75	70.05	73.48	126	125.28	125.4	5	1.63
Impact 4	150	151.88	149.26	36	41.02	33.28	5.36	2.82
Impact 5	150	147.52	149.09	96	93.06	94.72	3.85	1.57
Impact 6	205	202.53	206.52	104	107.29	103.1	4.11	1.77
Impact 7	255	250.35	256.93	154	152.53	154.74	4.88	2.07
Impact 8	305	301.78	306.82	74	75.85	73.55	3.71	1.87

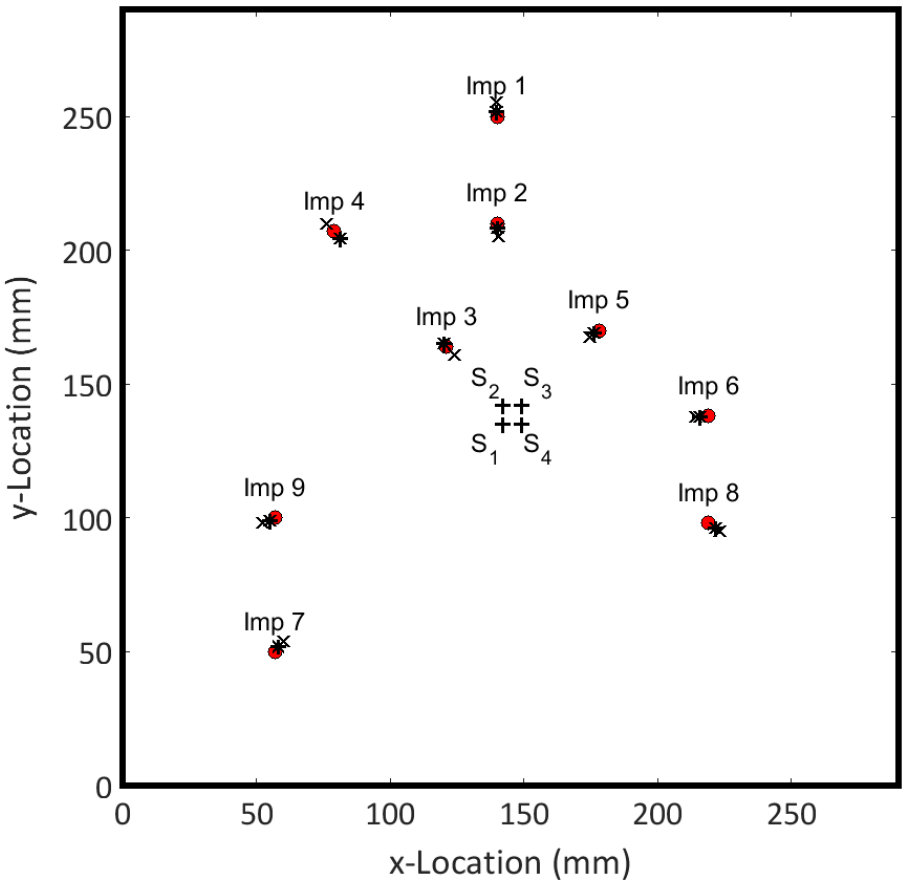

Figure 8. Source location results on the composite plate. The calculated impact positions are shown as a cross (×) for the CF-AIC picker, and as a star (∗) for the threshold AIC picker. The true impact positions are shown as a circle (∘).

Table 5. Impact positions and errors for the composite plate.

	X (mm, real value)	X (mm, detected value – CF AIC picker)	X (mm, detected value – threshold AIC picker)	Y (mm, real value)	Y (mm, detected value – CF AIC picker)	Y (mm, detected value – threshold AIC picker)	Location error Ψ (mm, CF AIC picker)	Location error Ψ (mm, threshold AIC picker)
Impact 1	140	139.7	139.9	250	255.46	251.81	5.47	1.81
Impact 2	140	140.38	140.17	210	205.29	208.24	4.73	1.77
Impact 3	121	124.1	119.95	164	160.71	165.05	4.52	1.48
Impact 4	79	76.18	81.31	207	209.9	204.39	4.05	3.49
Impact 5	178	174.58	176.12	170	167.54	169.11	4.21	2.08
Impact 6	219	214.27	215.84	138	137.63	137.59	4.74	3.19
Impact 7	57	59.99	58.22	50	53.73	51.8	4.78	2.17
Impact 8	219	223.26	221.46	98	95.02	96.06	5.2	3.13
Impact 9	57	52.46	54.96	100	98.14	98.99	4.91	2.28

With reference to Table 4 and Table 5, both AIC pickers are able to localise impacts with an accuracy described by a small location error Ψ less than 6 mm for both aluminium and composite samples.

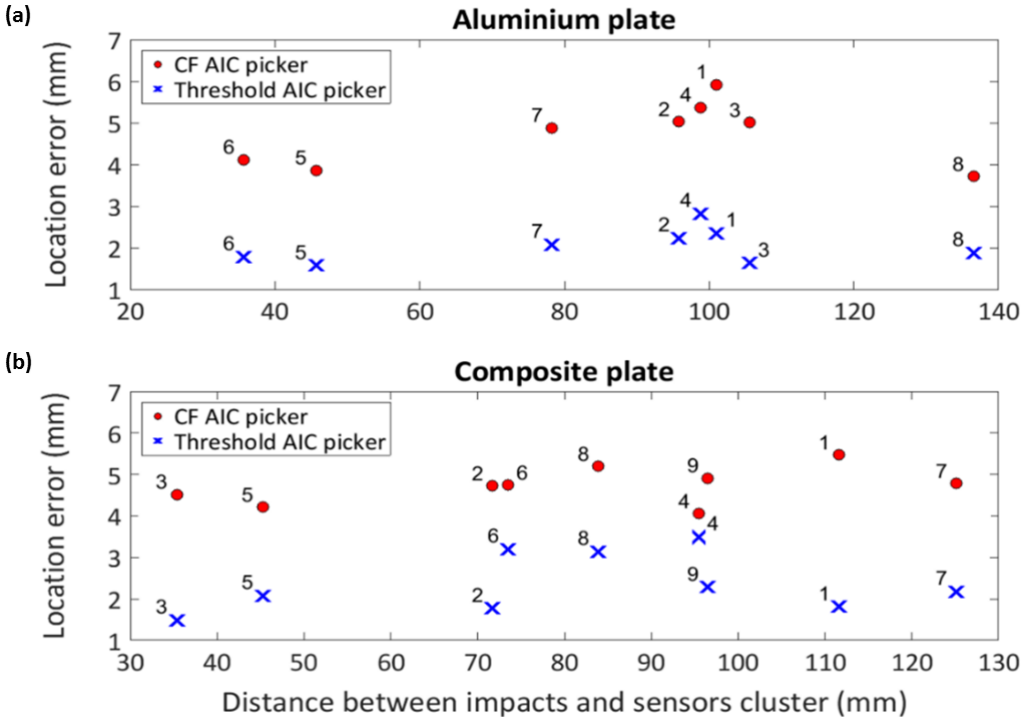

Figure 9. Localisation error using both the CF and threshold AIC methods for the impacts on the aluminium sample (a) and the composite plate (b).

In accordance with Tables 4 and 5, Figure 9 shows a summary of the impact localisation error Ψ as function of the distance between the impact point and the centre of sensor clusters for the aluminium and composite samples using both the standard AIC picker and the threshold one. As it can be seen from this figure, the threshold AIC method provided better results with a maximum localisation error less than 3 mm for the aluminium sample and less than 4 mm for the composite plate. However, it is difficult to find a clear trend of the localisation error increasing with the distance between the impact point and the sensors cluster location [see for instance the location errors of Impacts 3 and 8 in Figure 9(a) and of Impacts 4 and 9 in Figure 9(b)]. This could be due to undesired instrumentation effects such as the cross-talk in the receiving signals, which are independent from the localisation algorithm and may systematically affect the time of arrival estimation. Table 6 reports the wave velocities obtained from the impact localisation algorithm considering both TOAs calculation methods. Since the energy of each impact was the same, the order of magnitude of the wave velocity for each test specimen was very similar (see Table 6). This was an expected result that further confirms the validity of the proposed impact localisation algorithm.

Table 6. Wave velocities (m/s).

	Aluminium		Composite	
	CF AIC picker	threshold AIC picker	CF AIC picker	threshold AIC picker
Impact 1	2523.2	2555.2	1953.9	1952
Impact 2	2521.4	2577.7	1950.1	2044.4
Impact 3	2523.5	2522.1	1966.8	2041.7
Impact 4	2520.3	2520.8	1950.9	1955.4
Impact 5	2566.4	2574.8	1954.9	2049.8
Impact 6	2540.5	2573.7	1953	1953
Impact 7	2522.7	2576.8	1951.2	1959.4
Impact 8	2522.5	2578.1	1950.1	1950.3
Impact 9			2047.7	1957.4

6 CONCLUSIONS

A new linearised algorithm for the impact source localisation and wave velocity determination was here presented. It is based on the differences of the stress waves measured by four surface-bonded AE piezoelectric transducers. An optimal sensor configuration was used to linearise the systems of equations for the identification of the impact coordinates. The acquired signals were processed in order to determine the TOAs as an input of the proposed algorithm. Two different methods based on Akaike Information Criterion were performed to provide an accurate TOA results.

A number of experimental impact tests were performed on two different specimens, an aluminium and composite plate in order to validate the proposed methodology. Impact localisation results showed the validity of this algorithm, which was able to predict the impact point with high accuracy, i.e. with a maximum location error less than 4 mm by using the threshold AIC picker and with an impact error ranging between 4 and 6 mm by using the characteristic function AIC picker. Since the computational time of both AIC pickers is similar, the threshold one can be used for further TOA applications. This impact localisation method overcomes the limits of previous triangulation approaches as it does not need the knowledge of the material proprieties and the wave velocity. This could be embedded into an automatic impact localisation system that can be retrofitted on existing structures leading to more efficient inspection and enabling prediction of damage severity. By knowing impacts occurrence and location, would allow for a localized search, saving time and expense, and maintenance can be scheduled only when necessary.

REFERENCES

1. Balageas, D., Fritzen, C. P. and Güemes, A. (Eds.) (2010). Structural Health Monitoring. (Vol. 90). John Wiley & Sons.
2. Tobias, A. (1976). Acoustic-emission source location in two dimensions by an array of three sensors. *Non-destructive testing*, *9*(1), 9-12.
3. McLaskey, G. C., Glaser, S. D. and Grosse, C. U. (2010). Beamforming array techniques for acoustic emission monitoring of large concrete structures. *Journal of Sound and Vibration*, *329*(12), 2384-2394.
4. He, T., Pan, Q., Liu, Y., Liu, X. and Hu, D. (2012). Near-field beamforming analysis for acoustic emission source localization. *Ultrasonics*, *52*(5), 587-592.
5. Ciampa, F. And Meo, M. (2010). Acoustic emission source localization and velocity determination of the fundamental mode A_0 using wavelet analysis and a Newton-based optimization technique. *Smart Materials and Structures*, *19*(4), 045027.
6. Kundu, T., Das, S. and Jata, K. V. (2007). Point of impact prediction in isotropic and anisotropic plates from the acoustic emission data. *The Journal of the Acoustical Society of America*, *122*(4), 2057-2066.
7. Kundu, T., Das, S., Martin, S. A. and Jata, K. V. (2008). Locating point of impact in anisotropic fiber reinforced composite plates. *Ultrasonics*, *48*(3), 193-201.
8. Nakatani, H., Hajzargarbashi, T., Ito, K., Kundu, T. and Takeda, N. (2013). Locating point of impact on an anisotropic cylindrical surface using acoustic beamforming technique. In *Key Engineering Materials* (Vol. 558, pp. 331-340). Trans Tech Publications.
9. Seydel, R. and Chang, F. K. (2001). Impact identification of stiffened composite panels: I. System development. *Smart Materials and Structures*, *10*(2), 354-369.
10. Seydel, R. and Chang, F. K. (2001). Impact identification of stiffened composite panels: II. Implementation studies. *Smart materials and structures*, *10*(2), 370-379.
11. Meo, M., Zumpano, G., Piggott, M. and Marengo, G. (2005). Impact identification on a sandwich plate from wave propagation responses. *Composite structures*, *71*(3), 302-306.
12. Kurokawa, Y., Mizutani, Y. And Mayuzumi, M. (2005). Real-time executing source location system applicable to anisotropic thin structures. *Journal of Acoustic Emission*, *23*, 224-232.
13. Ciampa, F. and Meo, M. (2010). A new algorithm for acoustic emission localization and flexural group velocity determination in anisotropic structures. *Composites Part A: Applied Science and Manufacturing*, *41*(12), 1777-1786.
14. Ciampa, F., Meo, M. and Barbieri, E. (2012). Impact localization in composite structures of arbitrary cross

section. *Structural Health Monitoring*, *11*(6), 643-655.

15. Kundu, T. (2012, July). A new technique for acoustic source localization in an anisotropic plate without knowing its material properties. In *6th European Workshop on Structural Health Monitoring, Dresden, Germany*.
16. Kundu, T., Nakatani, H. and Takeda, N. (2012). Acoustic source localization in anisotropic plates. *Ultrasonics*, *52*(6), 740-746.
17. Tong, C. and Kennett, B. L. (1996). Automatic seismic event recognition and later phase identification for broadband seismograms. *Bulletin of the Seismological Society of America*, *86*(6), 1896-1909.
18. Baer, M. and Kradolfer, U. (1987). An automatic phase picker for local and teleseismic events. *Bulletin of the Seismological Society of America*, *77*(4), 1437-1445.
19. Kurz, J. H., Grosse, C. U. and Reinhardt, H. W. (2005). Strategies for reliable automatic onset time picking of acoustic emissions and of ultrasound signals in concrete. *Ultrasonics*, *43*(7), 538-546.
20. Ziola, S. M. and Gorman, M. R. (1991). Source location in thin plates using cross-correlation. *The Journal of the Acoustical Society of America*, *90*(5), 2551-2556.
21. Kosel, T., Grabec, I. and Kosel, F. (2003). Intelligent location of simultaneously active acoustic emission sources: Part I. *Aircraft Engineering and Aerospace Technology*, *75*(1), 11-17.
22. Dai, H. and MacBeth, C. (1997). The application of back-propagation neural network to automatic picking seismic arrivals from single-component recordings. *Journal of Geophysical Research: Solid Earth*, *102*(B7), 15105-15113.
23. Boschetti, F., Dentith, M. D. and List, R. D. (1996). A fractal-based algorithm for detecting first arrivals on seismic traces. *Geophysics*, *61*(4), 1095-1102.
24. Xu, J. (2011). P-wave onset detection based on the spectrograms of the AE signals. In *Advanced Materials Research* (Vol. 250, pp. 3807-3810). Trans Tech Publications.
25. Hinkley, D. V. (1971). Inference about the change-point from cumulative sum tests. *Biometrika*, *58*, 509-523.
26. Ciampa, F. and Meo, M. (2014). Impact localization on a composite tail rotor blade using an inverse filtering approach. *Journal of Intelligent Material Systems and Structures*, *25*(15), 1950-1958.
27. Ciampa, F., Boccardi, S. and Meo, M. (2016). Factors affecting the imaging of the impact location with inverse filtering and diffuse wave fields. *Journal of Intelligent Material Systems and Structures*, *27*(11), 1523-1533.
28. Akaike, H. (1973). Information theory and an extension of the maximum likelihood principle. In: BN Petrov, F Csaki, editors, *Second international symposium on information theory*, Springer-Verlag, 267-281.
29. Akaike, H. (1974). Markovian representation of stochastic processes and its application to the analysis of autoregressive moving average processes. *Annals of the Institute of Statistical Mathematics*, *26*(1), 363-387.

30. Akaike, H. (1974). A new look at the statistical model identification. *IEEE transactions on automatic control*, *19*(6), 716-723.

31. Kitagawa, G. and Akaike, H. (1978). A procedure for the modeling of non-stationary time series. *Annals of the Institute of Statistical Mathematics*, *30*(1), 351-363.

32. Yokota, T., Zhou, S., Mizoue, M. and Nakamura, I. (1981). An automatic measurement of arrival time of seismic waves and its application to an on-line processing system. *Bulletin of the Earthquake Research Institute*, *56*, 449-484.

33. Zhang, H., Thurber, C. and Rowe, C. (2003). Automatic P-wave arrival detection and picking with multiscale wavelet analysis for single-component recordings. *Bulletin of the Seismological Society of America*, *93*(5), 1904-1912.

34. Maeda, N. (1985). A method for reading and checking phase times in auto-processing system of seismic wave data. *Zisin*, *38*(3), 365-379.

35. Sleeman, R. and van Eck, T. (1999). Robust automatic P-phase picking: an on-line implementation in the analysis of broadband seismogram recordings. *Physics of the earth and planetary interiors*, *113*(1), 265-275.

36. Leonard, M. and Kennett, B. L. N. (1999). Multi-component autoregressive techniques for the analysis of seismograms. *Physics of the Earth and Planetary Interiors*, *113*(1), 247-263.

37. Sedlak, P., Hirose, Y., Khan, S. A., Enoki, M. and Sikula, J. (2009). New automatic localization technique of acoustic emission signals in thin metal plates. *Ultrasonics*, *49*(2), 254-262.

38. Sedlak, P., Hirose, Y. and Enoki, M. (2013). Acoustic emission localization in thin multi-layer plates using first-arrival determination. *Mechanical Systems and Signal Processing*, *36*(2), 636-649.

39. Carpinteri, A., Xu, J., Lacidogna, G. and Manuello, A. (2012). Reliable onset time determination and source location of acoustic emissions in concrete structures. *Cement and concrete composites*, *34*(4), 529-537.

40. Niccolini, G., Xu, J., Manuello, A., Lacidogna, G. and Carpinteri, A. (2012). Onset time determination of acoustic and electromagnetic emission during rock fracture. *Progress In Electromagnetics Research Letters*, *35*, 51-62.

41. Douglas, A. (1997). Bandpass filtering to reduce noise on seismograms: Is there a better way?. *Bulletin of the Seismological Society of America*, *87*(3), 770-777.

42. Allen, R. (1982). Automatic phase pickers: Their present use and future prospects. *Bulletin of the Seismological Society of America*, *72*(6B), S225-S242.

43. Paget, C. A., Atherton, K. and O'Brien, E. (2003). Triangulation algorithm for damage location in aeronautical composite structures. In *Proceedings of the 4th International Workshop on Structural Health Monitoring (F. Chang, ed.),(Stanford, CA, USA)*, 363-370.

APPENDIX

As described in Section 2.1 the reference sensor equation is:

$$(x_1 - x_I)^2 + (y_1 - y_I)^2 = \left(t_1 V_g\right)^2 \tag{A1}$$

and the final expressions for the four unknowns are:

$$\begin{cases} x_I = a_1 - {V_g}^2 c_1 \\ y_I = a_2 - {V_g}^2 c_2 \\ {V_g}^2 t_1 = a_3 - {V_g}^2 c_3 \end{cases} \tag{A2}$$

The aim is to obtain a third order equation with t_1 or V_g as unknown. The following procedure considers the reference time t_1 as unknown.

Substituting (A2) in (A1) we obtain:

$$\left[x_1 - \left(a_1 - \frac{a_3}{t_1 + c_3} c_1\right)\right]^2 + \left[y_1 - \left(a_2 - \frac{a_3}{t_1 + c_3} c_2\right)\right]^2 = {t_1}^2 \frac{a_3}{t_1 + c_3} \tag{A3}$$

that becomes, considering $t_1 + c_3 \neq 0$:

$$\begin{aligned} &\{x_1(t_1 + c_3) - a_1(t_1 + c_3) + a_3 c_1\}^2 + \{y_1(t_1 + c_3) - a_2(t_1 + c_3) + a_3 c_2\}^2 \\ &\qquad = {t_1}^2 (t_1 + c_3) a_3 \end{aligned} \tag{A4}$$

After some mathematical manipulation, equation (A4) can be written as:

$$\begin{aligned} &-a_3 {t_1}^3 + {t_1}^2 [(a_1 - x_1)^2 - a_3 c_3 + (a_2 - y_1)^2] \\ &\quad + t_1 [-2(a_1 - x_1)(a_3 c_1 - a_1 c_3 + x_1 c_3) - 2(a_2 - y_1)(a_3 c_2 - a_2 c_3 + y_1 c_3)] \\ &\quad + [(a_3 c_1 - a_1 c_3 + x_1 c_3)^2 + (a_3 c_2 - a_2 c_3 + y_1 c_3)^2] = 0 \end{aligned} \tag{A5}$$

or, in general, as reported below:

$$ {t_1}^3 Z_1 + {t_1}^2 Z_2 + t_1 Z_3 + Z_4 = 0 \tag{A6}$$

where the complete expressions of Z_i coefficients in (A6) are:

$$Z_1 = -a_3 \tag{A7}$$

$$Z_2 = (a_1 - x_1)^2 - a_3 c_3 + (a_2 - y_1)^2 \tag{A8}$$

$$Z_3 = -2(a_1 - x_1)(a_3 c_1 - a_1 c_3 + x_1 c_3) - 2(a_2 - y_1)(a_3 c_2 - a_2 c_3 + y_1 c_3) \tag{A9}$$

$$Z_4 = (a_3 c_1 - a_1 c_3 + x_1 c_3)^2 + (a_3 c_2 - a_2 c_3 + y_1 c_3)^2 \tag{A10}$$